The Astrophysical Journal Letters, 824:L28 (8pp), 2016 June 20 doi:10.3847/2041-8205/824/2/L28

LOWERING ICECUBE'S ENERGY THRESHOLD FOR POINT SOURCE SEARCHES IN THE SOUTHERN SKY

M. G. Aartsen[1], K. Abraham[2], M. Ackermann[3], J. Adams[4], J. A. Aguilar[5], M. Ahlers[6], M. Ahrens[7], D. Altmann[8], K. Andeen[9], T. Anderson[10], I. Ansseau[5], G. Anton[8], M. Archinger[11], C. Arguelles[12], T. C. Arlen[10], J. Auffenberg[13], X. Bai[14], S. W. Barwick[15], V. Baum[11], R. Bay[16], J. J. Beatty[17,18], J. Becker Tjus[19], K.-H. Becker[20], S. BenZvi[21], P. Berghaus[3], D. Berley[22], E. Bernardini[3], A. Bernhard[2], D. Z. Besson[23], G. Binder[16,24], D. Bindig[20], M. Bissok[13], E. Blaufuss[22], S. Blot[3], D. J. Boersma[25], C. Bohm[7], M. Börner[26], F. Bos[19], D. Bose[27], S. Böser[11], O. Botner[25], J. Braun[6], L. Brayeur[28], H.-P. Bretz[3], A. Burgman[25], N. Buzinsky[29], J. Casey[30], M. Casier[28], E. Cheung[22], D. Chirkin[6], A. Christov[31], K. Clark[32], L. Classen[8], S. Coenders[2], G. H. Collin[12], J. M. Conrad[12], D. F. Cowen[10,33], A. H. Cruz Silva[3], J. Daughhetee[30], J. C. Davis[17], M. Day[6], J. P. A. M. de André[34], C. De Clercq[28], E. del Pino Rosendo[11], H. Dembinski[35], S. De Ridder[36], P. Desiati[6], K. D. de Vries[28], G. de Wasseige[28], M. de With[37], T. DeYoung[34], J. C. Díaz-Vélez[6], V. di Lorenzo[11], H. Dujmovic[27], J. P. Dumm[7], M. Dunkman[10], B. Eberhardt[11], T. Ehrhardt[11], B. Eichmann[19], S. Euler[25], P. A. Evenson[35], S. Fahey[6], A. R. Fazely[38], J. Feintzeig[6], J. Felde[22], K. Filimonov[16], C. Finley[7], S. Flis[7], C.-C. Fösig[11], T. Fuchs[26], T. K. Gaisser[35], R. Gaior[39], J. Gallagher[40], L. Gerhardt[16,24], K. Ghorbani[6], L. Gladstone[6], M. Glagla[13], T. Glüsenkamp[3], A. Goldschmidt[24], G. Golup[28], J. G. Gonzalez[35], D. Góra[3], D. Grant[29], Z. Griffith[6], C. Ha[16,24], C. Haack[13], A. Haj Ismail[36], A. Hallgren[25], F. Halzen[6], E. Hansen[41], B. Hansmann[13], T. Hansmann[13], K. Hanson[6], D. Hebecker[37], D. Heereman[5], K. Helbing[20], R. Hellauer[22], S. Hickford[20], J. Hignight[34], G. C. Hill[1], K. D. Hoffman[22], R. Hoffmann[20], K. Holzapfel[2], A. Homeier[42], K. Hoshina[6,43], F. Huang[10], M. Huber[2], W. Huelsnitz[22], K. Hultqvist[7], S. In[27], A. Ishihara[39], E. Jacobi[3], G. S. Japaridze[44], M. Jeong[27], K. Jero[6], B. J. P. Jones[12], M. Jurkovic[2], A. Kappes[8], T. Karg[3], A. Karle[6], U. Katz[8], M. Kauer[6,45], A. Keivani[10], J. L. Kelley[6], J. Kemp[13], A. Kheirandish[6], M. Kim[27], T. Kintscher[3], J. Kiryluk[46], S. R. Klein[16,24], G. Kohnen[47], R. Koirala[35], H. Kolanoski[37], R. Konietz[13], L. Köpke[11], C. Kopper[29], S. Kopper[20], D. J. Koskinen[41], M. Kowalski[3,37], K. Krings[2], M. Kroll[19], G. Krückl[11], C. Krüger[6], J. Kunnen[28], S. Kunwar[3], N. Kurahashi[48], T. Kuwabara[39], M. Labare[36], J. L. Lanfranchi[10], M. J. Larson[41], D. Lennarz[34], M. Lesiak-Bzdak[46], M. Leuermann[13], J. Leuner[13], L. Lu[39], J. Lünemann[28], J. Madsen[49], G. Maggi[28], K. B. M. Mahn[34], S. Mancina[6], M. Mandelartz[19], R. Maruyama[45], K. Mase[39], H. S. Matis[24], R. Maunu[22], F. McNally[6], K. Meagher[5], M. Medici[41], M. Meier[26], A. Meli[36], T. Menne[26], G. Merino[6], T. Meures[5], S. Miarecki[16,24], E. Middell[3], L. Mohrmann[3], T. Montaruli[31], R. Nahnhauer[3], U. Naumann[20], G. Neer[34], H. Niederhausen[46], S. C. Nowicki[29], D. R. Nygren[24], A. Obertacke Pollmann[20], A. Olivas[22], A. Omairat[20], A. O'Murchadha[5], T. Palczewski[50], H. Pandya[35], D. V. Pankova[10], Ö. Penek[13], J. A. Pepper[50], C. Pérez de los Heros[25], C. Pfendner[17], D. Pieloth[26], E. Pinat[5], J. Posselt[20], P. B. Price[16], G. T. Przybylski[24], M. Quinnan[10], C. Raab[5], L. Rädel[13], M. Rameez[31], K. Rawlins[51], R. Reimann[13], M. Relich[39], E. Resconi[2], W. Rhode[26], M. Richman[48], B. Riedel[29], S. Robertson[1], M. Rongen[13], C. Rott[27], T. Ruhe[26], D. Ryckbosch[36], L. Sabbatini[6], A. Sandrock[26], J. Sandroos[11], S. Sarkar[41,52], K. Satalecka[3], M. Schimp[13], P. Schlunder[26], T. Schmidt[22], S. Schoenen[13], S. Schöneberg[19], A. Schönwald[3], L. Schumacher[13], D. Seckel[35], S. Seunarine[49], D. Soldin[20], M. Song[22], G. M. Spiczak[49], C. Spiering[3], M. Stahlberg[13], M. Stamatikos[17,53], T. Stanev[35], A. Stasik[3], A. Steuer[11], T. Stezelberger[24], R. G. Stokstad[24], A. Stößl[3], R. Ström[25], N. L. Strotjohann[3], G. W. Sullivan[22], M. Sutherland[17], H. Taavola[25], I. Taboada[30], J. Tatar[16,24], S. Ter-Antonyan[38], A. Terliuk[3], G. Tešić[10], S. Tilav[35], P. A. Toale[50], M. N. Tobin[6], S. Toscano[28], D. Tosi[6], M. Tselengidou[8], A. Turcati[2], E. Unger[25], M. Usner[3], S. Vallecorsa[31], J. Vandenbroucke[6], N. van Eijndhoven[28], S. Vanheule[36], M. van Rossem[6], J. van Santen[3], J. Veenkamp[2], M. Vehring[13], M. Voge[42], M. Vraeghe[36], C. Walck[7], A. Wallace[1], M. Wallraff[13], N. Wandkowsky[6], Ch. Weaver[29], C. Wendt[6], S. Westerhoff[6], B. J. Whelan[1], N. Whitehorn[16], S. Wickmann[13], K. Wiebe[11], C. H. Wiebusch[13], L. Wille[6], D. R. Williams[50], L. Wills[48], H. Wissing[22], M. Wolf[7], T. R. Wood[29], K. Woschnagg[16], D. L. Xu[6], X. W. Xu[38], Y. Xu[46], J. P. Yanez[3], G. Yodh[15], S. Yoshida[39], and M. Zoll[7]

(IceCube Collaboration)

[1] Department of Physics, University of Adelaide, Adelaide, 5005, Australia
[2] Physik-department, Technische Universität München, D-85748 Garching, Germany
[3] DESY, D-15735 Zeuthen, Germany
[4] Department of Physics and Astronomy, University of Canterbury, Private Bag 4800, Christchurch, New Zealand
[5] Université Libre de Bruxelles, Science Faculty CP230, B-1050 Brussels, Belgium
[6] Department of Physics and Wisconsin IceCube Particle Astrophysics Center, University of Wisconsin, Madison, WI 53706, USA; jacob.feintzeig@gmail.com
[7] Oskar Klein Centre and Department of Physics, Stockholm University, SE-10691 Stockholm, Sweden
[8] Erlangen Centre for Astroparticle Physics, Friedrich-Alexander-Universität Erlangen-Nürnberg, D-91058 Erlangen, Germany
[9] Department of Physics, Marquette University, Milwaukee, WI, 53201, USA
[10] Department of Physics, Pennsylvania State University, University Park, PA 16802, USA
[11] Institute of Physics, University of Mainz, Staudinger Weg 7, D-55099 Mainz, Germany
[12] Department of Physics, Massachusetts Institute of Technology, Cambridge, MA 02139, USA
[13] III. Physikalisches Institut, RWTH Aachen University, D-52056 Aachen, Germany
[14] Physics Department, South Dakota School of Mines and Technology, Rapid City, SD 57701, USA
[15] Department of Physics and Astronomy, University of California, Irvine, CA 92697, USA
[16] Department of Physics, University of California, Berkeley, CA 94720, USA
[17] Department of Physics and Center for Cosmology and Astro-Particle Physics, Ohio State University, Columbus, OH 43210, USA

[18] Department of Astronomy, Ohio State University, Columbus, OH 43210, USA
[19] Fakultät für Physik & Astronomie, Ruhr-Universität Bochum, D-44780 Bochum, Germany
[20] Department of Physics, University of Wuppertal, D-42119 Wuppertal, Germany
[21] Department of Physics and Astronomy, University of Rochester, Rochester, NY 14627, USA
[22] Department of Physics, University of Maryland, College Park, MD 20742, USA
[23] Department of Physics and Astronomy, University of Kansas, Lawrence, KS 66045, USA
[24] Lawrence Berkeley National Laboratory, Berkeley, CA 94720, USA
[25] Department of Physics and Astronomy, Uppsala University, Box 516, S-75120 Uppsala, Sweden
[26] Department of Physics, TU Dortmund University, D-44221 Dortmund, Germany
[27] Department of Physics, Sungkyunkwan University, Suwon 440-746, Korea
[28] Vrije Universiteit Brussel, Dienst ELEM, B-1050 Brussels, Belgium
[29] Department of Physics, University of Alberta, Edmonton, Alberta, Canada T6G 2E1
[30] School of Physics and Center for Relativistic Astrophysics, Georgia Institute of Technology, Atlanta, GA 30332, USA
[31] Département de physique nucléaire et corpusculaire, Université de Genève, CH-1211 Genève, Switzerland
[32] Department of Physics, University of Toronto, Toronto, Ontario, Canada, M5S 1A7
[33] Department of Astronomy and Astrophysics, Pennsylvania State University, University Park, PA 16802, USA
[34] Department of Physics and Astronomy, Michigan State University, East Lansing, MI 48824, USA
[35] Bartol Research Institute and Department of Physics and Astronomy, University of Delaware, Newark, DE 19716, USA
[36] Department of Physics and Astronomy, University of Gent, B-9000 Gent, Belgium
[37] Institut für Physik, Humboldt-Universität zu Berlin, D-12489 Berlin, Germany
[38] Department of Physics, Southern University, Baton Rouge, LA 70813, USA
[39] Department of Physics, Chiba University, Chiba 263-8522, Japan
[40] Department of Astronomy, University of Wisconsin, Madison, WI 53706, USA
[41] Niels Bohr Institute, University of Copenhagen, DK-2100 Copenhagen, Denmark
[42] Physikalisches Institut, Universität Bonn, Nussallee 12, D-53115 Bonn, Germany
[43] Earthquake Research Institute, University of Tokyo, Bunkyo, Tokyo 113-0032, Japan
[44] CTSPS, Clark-Atlanta University, Atlanta, GA 30314, USA
[45] Department of Physics, Yale University, New Haven, CT 06520, USA
[46] Department of Physics and Astronomy, Stony Brook University, Stony Brook, NY 11794-3800, USA
[47] Université de Mons, B-7000 Mons, Belgium
[48] Department of Physics, Drexel University, 3141 Chestnut Street, Philadelphia, PA 19104, USA; naoko@icecube.wisc.edu
[49] Department of Physics, University of Wisconsin, River Falls, WI 54022, USA
[50] Department of Physics and Astronomy, University of Alabama, Tuscaloosa, AL 35487, USA
[51] Department of Physics and Astronomy, University of Alaska Anchorage, 3211 Providence Drive, Anchorage, AK 99508, USA
[52] Department of Physics, University of Oxford, 1 Keble Road, Oxford OX1 3NP, UK
[53] NASA Goddard Space Flight Center, Greenbelt, MD 20771, USA
Received 2016 April 28; accepted 2016 May 12; published 2016 June 21

ABSTRACT

Observation of a point source of astrophysical neutrinos would be a "smoking gun" signature of a cosmic-ray accelerator. While IceCube has recently discovered a diffuse flux of astrophysical neutrinos, no localized point source has been observed. Previous IceCube searches for point sources in the southern sky were restricted by either an energy threshold above a few hundred TeV or poor neutrino angular resolution. Here we present a search for southern sky point sources with greatly improved sensitivities to neutrinos with energies below 100 TeV. By selecting charged-current ν_μ interacting inside the detector, we reduce the atmospheric background while retaining efficiency for astrophysical neutrino-induced events reconstructed with sub-degree angular resolution. The new event sample covers three years of detector data and leads to a factor of 10 improvement in sensitivity to point sources emitting below 100 TeV in the southern sky. No statistically significant evidence of point sources was found, and upper limits are set on neutrino emission from individual sources. A posteriori analysis of the highest-energy ($\sim$100 TeV) starting event in the sample found that this event alone represents a 2.8σ deviation from the hypothesis that the data consists only of atmospheric background.

Key words: astroparticle physics – neutrinos

1. INTRODUCTION

Despite 100 years of cosmic-ray observations, the sources of the highest energy cosmic rays remain unknown (Beatty & Westerhoff 2009; Kotera & Olinto 2011). Cosmic rays are predicted to be accelerated to very high energies in astrophysical objects, where they produce neutrinos upon interacting with matter or photons (Stecker et al. 1991; Waxman & Bahcall 1999; Learned & Mannheim 2000; Anchordoqui et al. 2014). The properties of neutrinos make them a unique astrophysical messenger. Interacting only via the weak force, they can travel astronomical distances without experiencing significant absorption. Neutral in charge, neutrinos follow straight paths through space even in magnetic fields, thus pointing back to their origin. Since high-energy cosmic neutrinos are only known to be produced in interactions of accelerated hadrons, observing neutrino point sources would identify cosmic-ray sources.

The IceCube Neutrino Observatory observed an excess of high-energy neutrinos that is consistent with a diffuse astrophysical neutrino flux (Aartsen et al. 2013a, 2014e, 2015a, 2015b). The origin of this flux remains unknown, and no significant clustering or correlation among the highest-energy events has been observed. Additional searches for point-source emission by IceCube and ANTARES using muon tracks have found neither evidence for point-like nor extended sources (Aartsen et al. 2014d, 2015c; Adrian-Martinez et al. 2014). A number of explanations for this flux have been proposed; see Anchordoqui et al. (2014) and references therein.

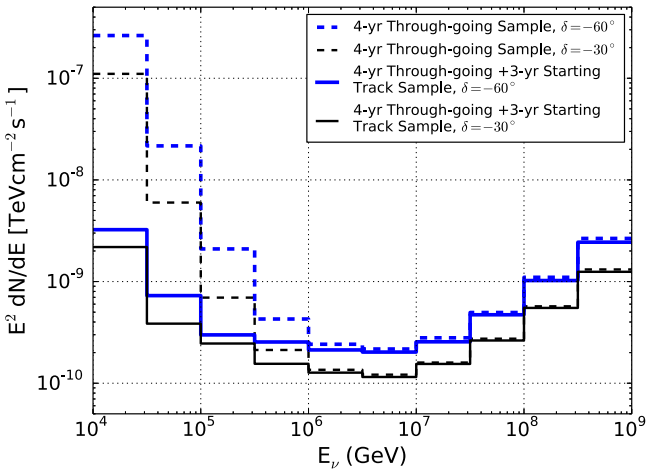

Figure 1. Discovery flux as a function of neutrino energy at a 5σ confidence level. Point sources with an E^{-2} spectrum are simulated over a half-decade in energy, and the flux in each bin required for discovery forms the curve above. Previous IceCube results (Aartsen et al. 2014d) are shown with dashed lines. The new event selection lowers the discovery threshold at 10^5 GeV by a factor of ∼10.

Potential sources of high-energy neutrinos include supernova remnants (SNRs; Cavasinni et al. 2006; Kistler & Beacom 2006; Gonzalez-Garcia et al. 2014), pulsars (Bednarek & Protheroe 1997; Link & Burgio 2005; Fang et al. 2012), active galactic nuclei (AGNs; Kalashev et al. 2013; Murase et al. 2014; Stecker et al. 1991), and starburst galaxies (Romero & Torres 2003; Loeb & Waxman 2006; Lacki et al. 2011). Many potential Galactic sources are in the southern sky and are predicted to accelerate cosmic rays to PeV energies, producing TeV–PeV neutrinos. Additionally, gamma-ray telescopes observe many Galactic sources with energy cutoffs below 100 TeV (Aharonian et al. 2006; Ackermann et al. 2013), suggesting Galactic neutrino emission may be most prominent in this energy range.

Southern sky point source searches with IceCube are difficult at these energies because atmospheric muons are backgrounds in this region of sky, triggering the detector at a rate of 2.5 kHz. They have a softer energy spectrum than the expected signal, and can be reduced by selecting well-reconstructed high-energy throughgoing tracks (Abbasi et al. 2009a; Aartsen et al. 2014d). This strategy increases the effective detector volume with neutrino-induced muons originating outside the detector, which can be reconstructed to $<1^\circ$. However, the large background requires a high-energy threshold, reducing the sensitivity below 1 PeV. An alternative strategy removes the atmospheric muon background by selecting high-energy contained-vertex events —bright events that start inside the detector (Aartsen et al. 2013a, 2014e, 2015a). This removes the majority of the background, providing a signal-dominated sample. However, most of these events are spherical light deposition from charged-current ν_e or ν_τ interactions or all-flavor neutral-current interactions. These events have $\sim 15^\circ$ angular resolutions, restricting their utility for point source searches.

The analysis presented here lowers IceCube's energy threshold in the southern sky by selecting charged-current ν_μ events that start inside the detector. Compared to the high-energy contained-vertex event search (Aartsen et al. 2014e), this enhances the ν_μ effective area below ∼200 TeV, thereby increasing the expected rate of signal events with $<1^\circ$ angular resolution. Compared to the throughgoing muon analysis (Aartsen et al. 2014d), the background rate is reduced by two orders of magnitude while retaining similar angular resolution, energy resolution, and neutrino effective area below ∼100 TeV. This selection provides a nearly independent event sample, which is combined with the throughgoing muon data in a joint likelihood fit.

2. EVENT SELECTION AND ANALYSIS TECHNIQUE

The IceCube Neutrino Observatory is a cubic-kilometer array of photomultiplier tubes (PMTs) embedded in the glacial ice at the geographic South Pole (Achterberg et al. 2006; Abbasi et al. 2009b). Eighty-six cables (called strings) are instrumented with 5160 PMTs, 1.5–2.5 km below the surface of the glacier. Neutrinos interact in the ice and produce charged leptons that are detected via their Cherenkov radiation by the PMTs (Abbasi et al. 2010). The analysis presented here searches for "starting tracks"—charged-current ν_μ events characterized by a large initial energy loss inside the detector followed by a track pattern as the resulting muon traverses and exits the detector. The dominant background for this search consists of atmospheric muons produced in air showers, a small fraction of which deposit little light upon entering the detector and therefore pass the starting track event selection. Atmospheric neutrinos form a subdominant background, but are indistinguishable from astrophysical neutrinos, unless a muon from the same air shower also reaches the detector (Schonert et al. 2009; Gaisser et al. 2014).

The starting track event selection is applied to data collected between 2010 and 2013. This includes one year of data from the 79-string detector configuration and two years from the completed 86-string detector. The event selection is performed using a two-stage veto. First, events with hits on the outer layer of the detector are removed using the veto algorithm from Aartsen et al. (2013a). The veto region includes the outer strings, the top 90 m and bottom 10 m of the detector, and a 60 m layer of PMTs in a region of dusty ice in the middle of the detector. Any event with more than two of its first 250 observed photoelectrons (PE) in the veto region is removed. Additionally, events with fewer than 1500 total PEs are removed. This leaves ∼3900 events per year, mostly atmospheric muons. In contrast, the search in Aartsen et al. (2013a) used the same veto criteria, but required events to deposit 6000 PE or greater, and found 37 events in the same data set.

Most remaining events still start closer to the border of the detector than expected for a collection of true starting events. This is an energy-dependent effect—high-energy background is more likely to emit observable light near the border, while low-energy background events can pass by a couple of strings without being detected. Two likelihood-based reconstructions are used. One estimates the position of the first energy loss by fitting for positions of stochastic losses along the track, and the other fits the muon energy loss along its track as a proxy for the total muon energy (Aartsen et al. 2014a). A two-dimensional cut on these quantities removes 95% of the remaining background while retaining 91% of simulated ν_μ drawn from an E^{-2} spectrum.

Additionally, poorly reconstructed events and upgoing events are removed. Events with unreliable directions, where two algorithms have poor agreement, cannot help identify point sources and are removed. Starting events in the upgoing region

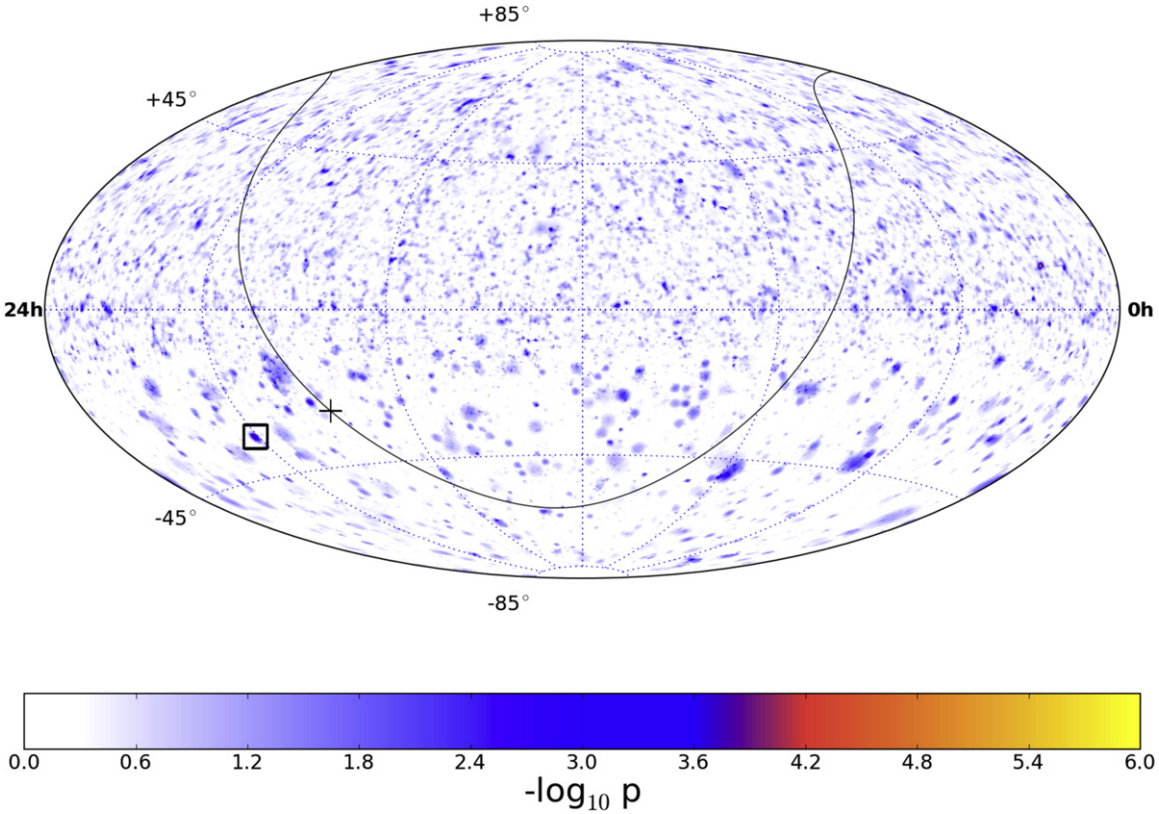

Figure 2. Pre-trial significance skymap in equatorial coordinates (J2000) for the starting track sample combined with the throughgoing muon sample. The black line indicates the Galactic plane, and the black plus sign indicates the Galactic center. In the southern sky, the most significant point is 301.15° R.A. and −34.15° decl., indicated with a box. The map in the northern sky is identical to Aartsen et al. (2014d).

(zenith angle >85°) are not included because the Earth and ice overburden in this range allow a sufficiently pure neutrino sample to be obtained with throughgoing events, as in the conventional point source samples (Aartsen et al. 2014d). After all cuts, the three-year event sample contains 549 events.

We search for point sources using the un-binned maximum likelihood method from Aartsen et al. (2013b, 2014d):

$$\mathcal{L}(\gamma, n_s) = \prod_j \mathcal{L}^j(\gamma, n_s^j) = \prod_j \prod_{i \in j} \left[\frac{n_s^j}{N^j} \mathcal{S}_i^j + \left(1 - \frac{n_s^j}{N^j}\right) \mathcal{B}_i^j \right]. \quad (1)$$

The first product is over the different data sets j, and $i \in j$ indicates that the ith event belongs to the jth data set. We combine the three-year starting track sample with the four-year throughgoing muon sample (Aartsen et al. 2014d), which includes data from partial IceCube configurations during construction. The number of neutrino events originating from the point source, n_s, and the spectral index for a source with a power-law spectrum, γ, are free parameters in the fit. The number of source events is the sum of the source events fitted within each data set, n_s^j. The ratios of the n_s^j are fixed by the relative number of signal events expected in each data set for the hypothesis being tested (point source at decl. δ with spectral index γ). The probability distribution functions (PDFs) $\mathcal{S}_i^j$ and $\mathcal{B}_i^j$ describe the spatial and energy distributions of the signal and background, respectively. Since our event sample mostly contains tracks, we apply the same energy and directional reconstructions used in Aartsen et al. (2014d), resulting in a median angular resolution below one degree for neutrinos with energies above 65 TeV.

We perform two hypothesis tests to search for point sources. The first is an all-sky likelihood scan, where the likelihood (Equation (1)) is maximized independently at each location in the sky on a 0.1° × 0.1° grid. The final results of this test are the location, best-fit parameters, and p-value of the most significant excess (the "hottest spot"). This is identical to Aartsen et al. (2014d), except we restrict our search for the hottest spot to decl. between −85° and −5°. The chance probability of finding a hottest spot as significant as the one observed is estimated by repeating the test on an ensemble of data sets randomized in R.A.

To reduce the large number of effective trials associated with scanning the entire sky, the second hypothesis test searches for neutrino emission from a catalog of candidate sources. These sources are selected based on multi-wavelength observations or astrophysical models predicting neutrino emission. We apply the same catalog used in the southern sky in Aartsen et al. (2014e), which contains 38 a priori-selected sources from previous IceCube and ANTARES analyses (Aartsen et al. 2014d; Adrian-Martinez et al. 2014). Similar to the all-sky search, the final post-trial p-value is obtained by repeating this test on randomized data sets.

Including the starting track sample leads to a substantial improvement in the discovery potential for point sources (Figure 1). For southern sky sources with a cutoff at 1 PeV, the discovery potential is a factor of two to three times better than previous results (Aartsen et al. 2014d). For sources with a cutoff at 100 TeV, the improvement is a factor of 10.

Table 1
Results of the a Priori Source List

Category	Source	R.A. (°)	Decl. (°)	$\hat{n}_s$	$\hat{\gamma}$	p-value	$\Phi^{90\%}_{\nu_\mu+\bar{\nu}_\mu}$
			Galactic Sources				
SNR	W28	270.43	−23.34	0.0	⋯	⋯	6.0
	RX J1713.7-3946	258.25	−39.75	0.0	⋯	⋯	10.4
	RX J0852.0-4622	133.0	−46.37	0.0	⋯	⋯	11.7
	RCW 86	220.68	−62.48	2.3	2.0	0.28	23.0
XB/mqso	LS 5039	276.56	−14.83	3.0	2.9	0.10	7.4
	GX 339-4	255.7	−48.79	1.7	1.9	0.41	17.0
	Cir X-1	230.17	−57.17	0.0	⋯	⋯	12.6
Pulsar/PWN	Vela X	128.75	−45.6	0.8	2.9	0.44	16.9
	HESS J1632-478	248.04	−47.82	0.0	⋯	⋯	11.6
	HESS J1616-508	243.78	−51.40	0.0	⋯	⋯	12.4
	HESS J1023-575	155.83	−57.76	0.5	1.7	0.46	17.8
	MSH 15-52	228.53	−59.16	0.0	⋯	⋯	12.9
	HESS J1303-631	195.74	−63.52	0.0	⋯	⋯	12.6
	PSR B1259-63	195.74	−63.52	0.0	⋯	⋯	12.6
	HESS J1356-645	209.0	−64.5	0.0	⋯	⋯	12.4
Galactic Center	Sgr A*	266.42	−29.01	0.0	⋯	⋯	7.6
Not Identified	HESS J1834-087	278.69	−8.76	0.0	⋯	⋯	2.0
	HESS J1741-302	265.25	−30.2	0.0	⋯	⋯	8.1
	HESS J1503-582	226.46	−58.74	0.0	⋯	⋯	13.2
	HESS J1507-622	226.72	−62.34	0.0	⋯	⋯	13.5
			Extragalactic Sources				
BL Lac	1ES 0347-121	57.35	−11.99	0.0	⋯	⋯	2.9
	1ES 1101-232	165.91	−23.49	0.0	⋯	⋯	5.9
	PKS 2155-304	329.72	−30.22	0.0	⋯	⋯	7.9
	H 2356-309	359.78	−30.63	0.0	⋯	⋯	8.2
	PKS 0548-322	87.67	−32.27	0.0	⋯	⋯	8.7
	PKS 0426-380	67.17	−37.93	0.0	⋯	⋯	10.3
	PKS 0537-441	84.71	−44.08	0.0	⋯	⋯	11.2
	PKS 2005-489	302.37	−48.82	0.0	⋯	⋯	11.8
FSRQ	3C279	194.05	−5.79	0.0	⋯	⋯	1.3
	HESS J1837-069	279.41	−6.95	0.0	⋯	⋯	1.4
	QSO 2022-077	306.42	−7.64	0.9	1.9	0.46	1.9
	PKS 1406-076	212.24	−7.87	6.3	2.6	0.10	3.3
	PKS 0727-11	112.58	−11.7	4.7	3.4	0.18	4.7
	QSO 1730-130	263.26	−13.08	2.4	3.9	0.28	4.9
	PKS 0454-234	74.27	−23.43	0.0	⋯	⋯	5.8
	PKS 1622-297	246.53	−29.86	4.1	2.5	0.19	14.3
	PKS 1454-354	224.36	−35.65	0.0	⋯	⋯	9.4
Radio Galaxies	Cen A	201.37	−43.02	0.0	⋯	⋯	11.5
Seyfert	ESO 139-G12	264.41	−59.94	0.0	⋯	⋯	12.4

Note. Galactic sources are grouped according to their classification as high-mass X-ray binaries or micro-quasars (HMXB/mqso), SNRs, pulsar wind nebulas (PWNs), star formation regions and unidentified sources. Extragalactic sources are grouped according to their classification as BL Lac objects, radio galaxies, flat-spectrum radio quasars (FSRQ) and starburst galaxies. The p-value is the (pre-trial) probability for each source direction to have a more significant excess due to background fluctuations. The $\hat{n}_S$ and $\hat{\gamma}$ columns give the best-fit number of signal events and spectral index of a power-law spectrum. When $\hat{n}_S = 0$, no p-value or $\hat{\gamma}$ are reported. The last column shows the $\nu_\mu + \bar{\nu}_\mu$ flux normalization classical upper limits (Neyman 1937) for an unbroken E^{-2} flux in units of 10^{-12} TeV^{-1} cm^{-2} s^{-1}.

3. RESULTS

The results from both tests are consistent with the background-only hypothesis. The skymap of pre-trial p-values is shown in Figure 2. In the southern sky, the skymap appears sparser because we observe only 549 starting track events. In the joint likelihood fit, the much lower background of the starting track sample suppresses fluctuations seen in the throughgoing sample, which has 100 times greater background.

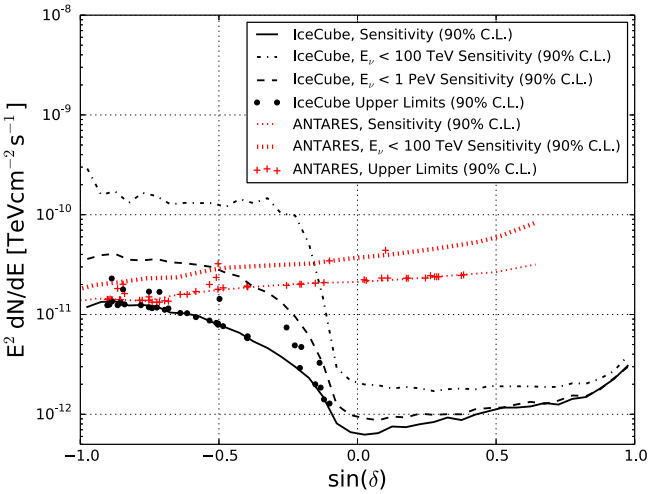

Figure 3. Muon neutrino upper limits (90% C.L.) evaluated for 38 sources (dots), for the three-year starting track sample combined with the four-year throughgoing muon sample. The solid black line is the median 90% C.L. upper limit or sensitivity for a point source with an unbroken E^{-2} spectrum. The sensitivities to E^{-2} spectra ending (with a sharp cutoff) at 1 PeV and 100 TeV are shown in the black dashed and dashed–dotted lines, respectively. The ANTARES (1338 days livetime) upper limits and sensitivities for two spectral hypotheses are shown in red (Adrian-Martinez et al. 2014).

The location of the most significant pre-trial p-value is 301.15° R.A. and −34.15° decl., where one starting track event is coincident with a small excess of events from the throughgoing muon sample. The likelihood fits 6.97 signal events with an $E^{-2.15}$ energy spectrum, resulting in a pre-trial p-value of 9.3×10^{-5}. Accounting for the trial factor associated with searching every location in the southern sky, the post-trial p-value is 0.97.

Results for the a priori source list search are shown in Table 1. The source with the strongest excess is the Galactic X-ray binary LS 5039, with a pre-trial p-value of 0.10. Accounting for the trial factor associated with the 38 sources on the list, the post-trial p-value is 0.76. Figure 3 shows the 90% confidence level upper limits and sensitivity on the E^{-2} neutrino flux from each source at its corresponding decl. Also shown is the analysis sensitivity, along with results from ANTARES (Adrian-Martinez et al. 2014).

Since the background is estimated by scrambling the detector data in R.A., the p-values are independent of theoretical uncertainties in the fluxes of atmospheric backgrounds as well as systematic uncertainties in the detector simulation. However, upper limits and analysis sensitivities are calculated by simulating the detector response to astrophysical neutrinos and are subject to these uncertainties. Using a detector simulation, the systematic uncertainties in the optical properties of the ice and the efficiency of the optical modules were estimated to have a 16% and 15% effect on the analysis sensitivity, respectively. Summing these uncorrelated errors in quadrature gives a 22% overall systematic uncertainty on the quoted sensitivities and upper limits, similar to that found in Aartsen et al. (2014d).

4. DISCUSSION

4.1. Constraints on Neutrino Emission Models

While Figure 3 shows upper limits for the E^{-2} neutrino flux from a variety of sources, many models predict fluxes with complex spectra. For example, the Galactic center has been the subject of recent neutrino emission models and discussion (Razzaque 2013; Supanitsky 2013; Anchordoqui et al. 2014; Gonzalez-Garcia et al. 2014). This is spurred not only by electromagnetic observations (Morris & Serabyn 1996; Carretti et al. 2013; Yoast-Hull et al. 2014), but also by the observation of high-energy astrophysical neutrinos (Aartsen et al. 2014e). The analysis presented here places constraints on the most optimistic possibilities. Gonzalez-Garcia et al. (2014) calculated that a point source with an unbroken E^{-2} power-law energy spectrum and flux normalization of 6×10^{-11} TeV^{-1} cm^{-2} s^{-1} at 1 TeV could be responsible for the high-energy neutrino events near the Galactic center. This flux is eight times greater than the Galactic center upper limit presented here. Even if the E^{-2} neutrino spectrum cuts off at 1 PeV, it is still excluded at 90% by this analysis, although an extended source could evade detection. On the other hand, the majority of models based on gamma-ray observations for this and other Galactic sources predict lower fluxes, many with spectral cutoffs below 100 TeV (Kistler & Beacom 2006; Kappes et al. 2007; Fox et al. 2013). Model tests of these fluxes lead to upper limits that are generally a factor of 10 or more above predictions.

4.2. A Posteriori Investigation of the Hottest Spot in the Skymap

While the hottest spot in the skymap was consistent with a background fluctuation, a single starting track event was the main contributor to the significance at this location. The event appears to be a high-energy ν_μ interacting inside the detector volume. The reconstructed vertex of this event is 286 m inside the detector, and it passes through three layers of PMTs that observe no photons. This event deposited 84 TeV (electromagnetic equivalent) inside the detector, which sets a strict lower bound on the neutrino energy (Aartsen et al. 2014a). When reconstructed as a throughgoing track, the reconstructed muon energy proxy for this event is 124 TeV, the highest in the starting event sample. Its reconstructed direction is 301.7° R.A. and −34.3° decl. with an estimated angular uncertainty of 0.6°, and its arrival time in MJD is 56093.1796492. This event was not found in Aartsen et al. (2014e) because its deposited charge is below the threshold for that analysis.

At this energy and zenith angle, the expected atmospheric ν_μ background is greatly suppressed by the atmospheric neutrino self-veto effect (Schonert et al. 2009; Gaisser et al. 2014). In the a posteriori analysis described here, we characterize the distribution of expected background events in zenith and energy to estimate the significance of having at least one event similar to the one observed in the data set.

To calculate the total expected background rate, we generate a PDF for astrophysical ν_μ signal and atmospheric ν_μ background as a function of reconstructed zenith and energy. We then take the ratio of these two PDFs to determine the signal to background likelihood ratio for this event's zenith and energy (Figure 4). The total atmospheric ν_μ background rate is then the rate of simulated events with a higher likelihood ratio. The total rate of such atmospheric events is 0.0022 in three years of livetime. This event therefore represents a 2.8σ deviation from the hypothesis that it is an atmospheric background.

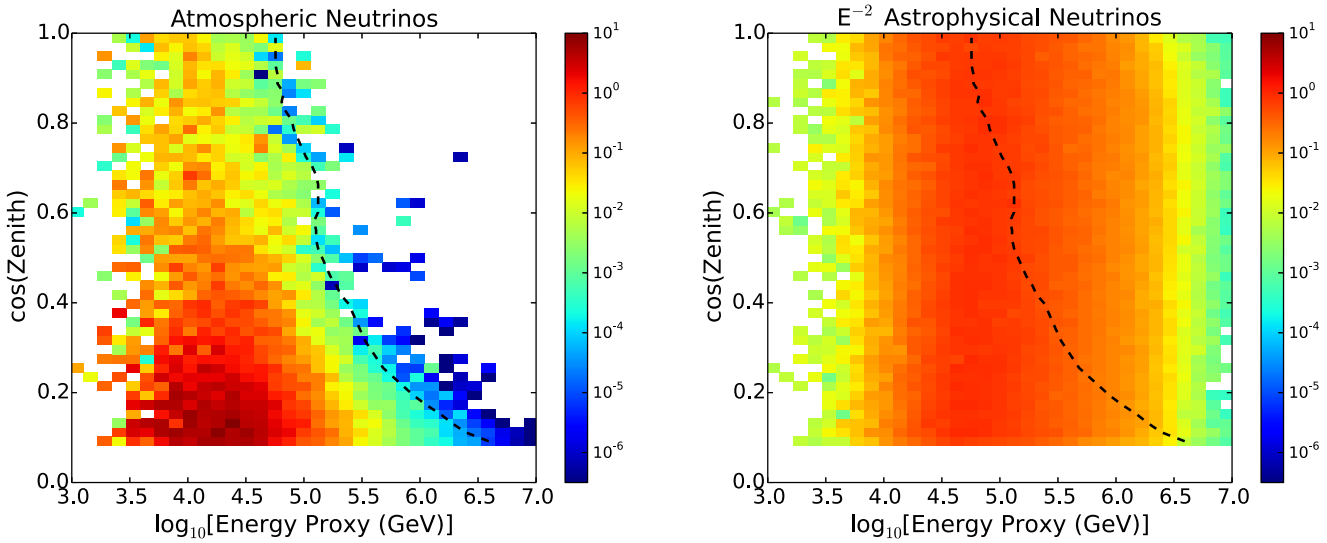

Figure 4. Atmospheric ν_μ background and astrophysical signal PDFs. The left plot shows the PDF as a function of reconstructed zenith angle and reconstructed energy for atmospheric neutrinos following models from Honda et al. (2007), Enberg et al. (2008), Gaisser (2013), and Aartsen et al. (2014c). This includes the self-veto probability from Gaisser et al. (2014) for each event. The right plot shows the PDF for E^{-2} astrophysical neutrinos. The likelihood ratio between the signal and background hypothesis is calculated for the observed event's energy and zenith, and the dashed line denotes the zenith-energy contour with this likelihood ratio. Events to the right of this contour are more "signal-like" than the observed event.

Atmospheric muons are a less likely candidate. Muons were simulated with directions, energies, and positions similar to the observed event. The expected rate of atmospheric muons that appear similar to the observed event is estimated to be less than 0.0001 events in three years, an order of magnitude lower than the atmospheric neutrino background.

While this event cannot be easily explained with the background hypothesis, it is consistent with an astrophysical signal hypothesis. The best-fit astrophysical neutrino flux measured in Aartsen et al. (2014e) would produce 4.1 starting track events in this data set, including 1.0 events with a muon energy proxy $\geqslant$124 TeV. Simulated signal events with similar reconstructed energies had primary neutrino energies of a few hundred TeV, most of which are carried out of the detector by the muon.

It is important to note the 2.8σ significance represents the chance probability that this event originates from an atmospheric flux. It does not include information about its spatial clustering with other events or its correlation with known astrophysical sources. Because there is no significant evidence for clustering nor correlation, this event does not represent the identification of a neutrino point source.

5. CONCLUSION

A new event selection technique presented here extends IceCube's sensitivity to southern sky point sources in the energy region below 100 TeV. No indication of a statistically significant source was found. Future analyses will probe fainter and lower energy sources in the southern sky by extending this technique further. Joint analyses with ANTARES (Adrian-Martinez et al. 2015) and future kilometer- and multi-kilometer-scale telescopes (Bagley et al. 2011; Aartsen et al. 2014b) will also push sensitivities in this region of the sky.

We acknowledge the support from the following agencies: U.S. National Science Foundation-Office of Polar Programs, U.S. National Science Foundation-Physics Division, University of Wisconsin Alumni Research Foundation, the Grid Laboratory Of Wisconsin (GLOW) grid infrastructure at the University of Wisconsin—Madison, the Open Science Grid (OSG) grid infrastructure; U.S. Department of Energy, and National Energy Research Scientific Computing Center, the Louisiana Optical Network Initiative (LONI) grid computing resources; Natural Sciences and Engineering Research Council of Canada, WestGrid and Compute/Calcul Canada; Swedish Research Council, Swedish Polar Research Secretariat, Swedish National Infrastructure for Computing (SNIC), and Knut and Alice Wallenberg Foundation, Sweden; German Ministry for Education and Research (BMBF), Deutsche Forschungsgemeinschaft (DFG), Helmholtz Alliance for Astroparticle Physics (HAP), Research Department of Plasmas with Complex Interactions (Bochum), Germany; Fund for Scientific Research (FNRS-FWO), FWO Odysseus programme, Flanders Institute to encourage scientific and technological research in industry (IWT), Belgian Federal Science Policy Office (Belspo); University of Oxford, United Kingdom; Marsden Fund, New Zealand; Australian Research Council; Japan Society for Promotion of Science (JSPS); the Swiss National Science Foundation (SNSF), Switzerland; National Research Foundation of Korea (NRF); Villum Fonden, Danish National Research Foundation (DNRF), Denmark.

REFERENCES

Aartsen, M., Abbasi, R., Abdou, Y., et al. 2013a, Sci, 342, 1242856
Aartsen, M., Abbasi, R., Abdou, Y., et al. 2013b, ApJ, 779, 132
Aartsen, M., Abbasi, R., Ackermann, M., et al. 2014a, JInst, 9, P03009
Aartsen, M., Abbasi, R., Ackermann, M., et al. 2014c, PhRvD, 89, 062007
Aartsen, M., Abraham, K., Ackermann, M., et al. 2015b, PhRvL, 115, 081102
Aartsen, M., Ackermann, M., Adams, J., et al. 2014b, arXiv:1412.5106
Aartsen, M., Ackermann, M., Adams, J., et al. 2014d, ApJ, 796, 109
Aartsen, M., Ackermann, M., Adams, J., et al. 2015a, PhRvD, 91, 022001
Aartsen, M., Ackermann, M., Adams, J., et al. 2015c, ApJ, 807, 46
Aartsen, M. G., Ackermann, M., Adams, J., et al. 2014e, PhRvL, 113, 101101
Abbasi, R., Abdou, Y., Abu-Zayyad, T., et al. 2009a, PhRvL, 103, 221102
Abbasi, R., Abdou, Y., Abu-Zayyad, T., et al. 2010, NIMPA, A618, 139

Abbasi, R., Ackermann, M., Adams, J., et al. 2009b, NIMPA, A601, 294
Achterberg, A., Ackermann, M., Adams, J., et al. 2006, APh, 26, 155
Ackermann, M., Ajello, M., Allafort, A., et al. 2013, Sci, 339, 807
Adrian-Martinez, S., Albert, A., Andre, M., et al. 2014, ApJL, 786, L5
Adrian-Martinez, S., Albert, A., Andre, M., et al. 2015, ApJ, submitted (arXiv:1511.02149)
Aharonian, F., Akhperjanian, A., Bazer-Bachi, A., et al. 2006, A&A, 449, 223
Anchordoqui, L. A., Barger, V., Cholis, I., et al. 2014, JHEAp, 1, 1
Bagley, P., Craig, J., Holford, A., et al. 2011, KM3NeT Technical Design Report for a Deep-Sea Research Infrastructure 299 Incorporating a Very Large Volume Neutrino Telescope (KM3NeT Consortium), http://km3net.org/TDR/TDRKM3NeT.pdf
Beatty, J. J., & Westerhoff, S. 2009, ARNPS, 59, 319
Bednarek, W., & Protheroe, R. 1997, PhRvL, 79, 2616
Carretti, E., Crocker, R. M., Staveley-Smith, L., et al. 2013, Natur, 493, 66
Cavasinni, V., Grasso, D., & Maccione, L. 2006, APh, 26, 41
Enberg, R., Reno, M. H., & Sarcevic, I. 2008, PhRvD, 78, 043005
Fang, K., Kotera, K., & Olinto, A. V. 2012, ApJ, 750, 118
Fox, D., Kashiyama, K., & Mszars, P. 2013, ApJ, 774, 74
Gaisser, T. K. 2013, EPJWC, 52, 9004
Gaisser, T. K., Jero, K., Karle, A., & van Santen, J. 2014, PhRvD, 90, 023009
Gonzalez-Garcia, M., Halzen, F., & Niro, V. 2014, APh, 57-58, 39
Honda, M., Kajita, T., Kasahara, K., Midorikawa, S., & Sanuki, T. 2007, PhRvD, 75, 043006
Kalashev, O. E., Kusenko, A., & Essey, W. 2013, PhRvL, 111, 041103
Kappes, A., Hinton, J., Stegmann, C., & Aharonian, F. A. 2007, ApJ, 656, 870
Kistler, M. D., & Beacom, J. F. 2006, PhRvD, 74, 063007
Kotera, K., & Olinto, A. V. 2011, ARA&A, 49, 119
Lacki, B. C., Thompson, T. A., Quataert, E., Loeb, A., & Waxman, E. 2011, ApJ, 734, 107
Learned, J. G., & Mannheim, K 2000, ARNPS, 50, 679
Link, B., & Burgio, F. 2005, PhRvL, 94, 181101
Loeb, A., & Waxman, E. 2006, JCAP, 0605, 003
Morris, M., & Serabyn, E. 1996, ARA&A, 34, 645
Murase, K., Inoue, Y., & Dermer, C. D. 2014, PhRvD, 90, 023007
Neyman, J. 1937, RSPTA, 236, 333
Razzaque, S. 2013, PhRvD, 88, 081302
Romero, G. E., & Torres, D. F. 2003, ApJL, 586, L33
Schonert, S., Gaisser, T. K., Resconi, E., & Schulz, O. 2009, PhRvD, 79, 043009
Stecker, F. W., Done, C., Salamon, M. H., & Sommers, P. 1991, PhRvL, 66, 2697
Supanitsky, A. 2013, arXiv:1312.7304
Waxman, E., & Bahcall, J. N. 1999, PhRvD, 59, 023002
Yoast-Hull, T. M., Gallagher, J., & Zweibel, E. G. 2014, arXiv:1405.7059